SCIENCE CHINA
Technological Sciences

•Article•

March 2024 Vol.67 No.3: 863–877
https://doi.org/10.1007/s11431-023-2443-8

A unified stochastic damage model for concrete based on multi-scale energy dissipation analysis

GUO ChengGong[1] & LI Jie[1,2*]

[1] College of Civil Engineering, Tongji University, Shanghai 200092, China;
[2] State Key Laboratory of Disaster Reduction in Civil Engineering, Shanghai 200092, China

Received February 11, 2023; accepted June 5, 2023; published online February 19, 2024

This work proposes a unified damage model for concrete within the framework of stochastic damage mechanics. Based on the micro-meso stochastic fracture model (MMSF), the nonlinear energy dissipation process of the microspring from nanoscale to microscale is investigated. In nanoscale, the rate process theory is adopted to describe the crack growth rate; therefore, the corresponding energy dissipation caused by a representative crack propagation can be obtained. The scale gap from nanoscale to microscale is bridged by a crack hierarchy model. Thus, the total energy dissipated by all cracks from the nanoscale to the microscale is gained. It is found that the fracture strain of the microspring can be derived from the above multi-scale energy dissipation analysis. When energy dissipation is regarded as some microdamage to the microspring, the constitutive law of the microspring is no longer linearly elastic, as previously assumed. By changing the expression of the damage evolution law from fracture strain to energy dissipation threshold, the new damage evolution model is derived. The proposed model can not only replicate the original static model but also extend to cases of rate dependence. By deriving the fracture strain under different strain rates, the rate sensitivity of concrete materials can be reflected. The model parameters can be conveniently obtained by identifying them with experimental data. Finally, several numerical examples are presented to verify the proposed model.

concrete damage model, stochastic damage, rate dependent, energy dissipation

Citation: Guo C G, Li J. A unified stochastic damage model for concrete based on multi-scale energy dissipation analysis. Sci China Tech Sci, 2024, 67: 863–877, https://doi.org/10.1007/s11431-023-2443-8

1 Introduction

As a heterogeneous composite, concrete exhibits complex mechanical behaviors under external forces. In the scope of continuum damage mechanics (CDM), the thermodynamically consistent continuum damage framework has been established owing to the efforts of previous work [1–8]. The main mechanical behaviors, such as strength softening, stiffness degradation, and the unilateral effect, can be rationally reflected. However, irreversible thermodynamics only provides the necessary condition for the damage evolution law through the Clausius-Duhamel inequality. In addition, concrete is a random medium in nature, and the microcracks in concrete are randomly distributed. Therefore, the damage evolution of concrete is bound to have inherent randomness, which cannot be revealed in the above deterministic framework.

Furthermore, the mechanical properties of concrete, like strength and fracture energy, are sensitive to strain rates [9,10]. Interestingly, no rate-sensitivity phenomenon is observed for linear elastic materials or materials in the linear elastic range [11]. This demonstrates the significant association between damage growth and the strain rate effect. The physical mechanism of rate sensitivity is still ambiguous [12]. Several theories, including the viscous effect [13,14] and the inertial effect [15,16], are proposed to explain the strain rate issue. As a result, dynamic damage models based on viscous theory [17–19] and inertial effects [20,21] for

*Corresponding author (email: lijie@tongji.edu.cn)

describing the dynamic properties of concrete have been developed. Despite some advancements in these models, it is still unclear how the dynamic properties of concrete relate to one another. In addition, few studies have considered the influence of the randomness of concrete.

Research on the random properties of concrete materials began in the 1980s [22]. The damage variable is defined as the fracture probability of the fiber bundles, which is essentially a deterministic result. Thereafter, Kandarpa et al. [23] improved the model by taking into account the correlation between the microsprings. The analytical expressions of mean and standard deviation for stochastic damage can be derived. According to the idea of stochastic damage, Li and his colleagues [24,25] proposed the micro-meso stochastic fracture model (MMSF) by taking into account two damage mechanisms (tension and shear). The model assumes that shear mechanisms are primarily responsible for controlling concrete failure under compressive stress. The MMSF was further extended to multi-dimensional cases through energy equivalent strain [25]. The assumption of random media [26,27] forms the foundation of the stochastic damage concept. That means the hydrated cement paste, aggregate, and interfacial transition zone in concrete can be regarded as single random media. Such a hypothesis has recently been supported by nano- and microscale experiments [28]. These progresses related to MMSF provide a unified framework to reflect the nonlinearity and randomness behaviors of concrete simultaneously.

In the MMSF, the constitutive law of the microspring is assumed to be linear elastic. It means there is no energy dissipation within the microspring before fracture, which may be inconsistent with the physical facts. The aim of this work is to reveal the nonlinear degradation constitutive law of the microspring during the loading process. Inspired by the work of Ding and Li [29], the multi-scale nonlinear energy dissipation process of the microspring is investigated in this paper. In this study, it was found that the fracture strain of the microspring corresponds to a certain energy dissipation limit. Therefore, a new MMSF can be established based on the energy dissipation analysis. Furthermore, the new model can be extended to rate-dependent situations by deriving the fracture strain under various strain rates. Dynamic fracture strain serves as the foundation for the relationship between dynamic properties like strength, elastic modulus, and fracture energy. In light of these results, a damage model is presented that can be employed for both static and dynamic loading. This model can be extended to account for fatigue loading, which will be developed in the following paper.

2 Deterministic elastoplastic damage framework

2.1 Damage variables

By applying the strain equivalence hypothesis [30], the damaged part can be separated from the effective stress space:

$$\boldsymbol{\sigma} = (\mathbb{I} - \mathbb{D}) : \overline{\boldsymbol{\sigma}}, \tag{1}$$

where $\boldsymbol{\sigma}$ and $\overline{\boldsymbol{\sigma}}$ are the Cauchy stress tensor and effective stress tensor, respectively; $\mathbb{D}$ is the fourth-order damage tensor; and $\mathbb{I}$ is the fourth-order identity tensor.

Owing to the significant difference between the uniaxial tensile strength and compressive strength of concrete, the stress decomposition concept [4,5] is widely adopted in constitutive modeling [27]:

$$\overline{\boldsymbol{\sigma}} = \overline{\boldsymbol{\sigma}}^{+} + \overline{\boldsymbol{\sigma}}^{-}, \tag{2}$$

where

$$\begin{cases} \overline{\boldsymbol{\sigma}}^{+} = \mathbb{P}^{+} : \overline{\boldsymbol{\sigma}}, \\ \overline{\boldsymbol{\sigma}}^{-} = \mathbb{P}^{-} : \overline{\boldsymbol{\sigma}}. \end{cases} \tag{3}$$

The expressions of the projection tensors $\mathbb{P}^{\pm}$ are

$$\begin{cases} \mathbb{P}^{+} = \sum_{a=1}^{3} H(\sigma_a) n^{(a)} \otimes n^{(a)} \otimes n^{(a)} \otimes n^{(a)}, \\ \mathbb{P}^{-} = \mathbb{I} - \mathbb{P}^{+}, \end{cases} \tag{4}$$

where σ_a and $n^{(a)}$ are the a-th eigenvalue and eigenvector of the effective stress tensor $\overline{\boldsymbol{\sigma}}$, respectively, and $H(\cdot)$ is the Heaviside function.

In the meantime, two damage variables d^{+} and d^{-} are introduced, where d^{+} and d^{-} correspond to the damage state related to tensile stress state and compressive stress state, respectively. The damage tensor is written as

$$\mathbb{D} = d^{+}\mathbb{P}^{+} + d^{-}\mathbb{P}^{-}. \tag{5}$$

The irreversible thermodynamics suggests that the energy conjugated force should be taken as the driving force of the internal variables. Therefore, Helmholtz free energy can be described as

$$\Psi = (1 - d^{+})\Psi_0^{+} + (1 - d^{-})\Psi_0^{-}, \tag{6}$$

where Ψ_0^{+} and Ψ_0^{-} are the positive and negative parts of the initial Helmholtz free energy, respectively.

The damage energy release rates Y^{+} and Y^{-} are defined as the energy conjugated forces of the damage variables:

$$\begin{cases} Y^{+} = -\dfrac{\partial \Psi}{\partial d^{+}} = \Psi_0^{+}, \\ Y^{-} = -\dfrac{\partial \Psi}{\partial d^{-}} = \Psi_0^{-}. \end{cases} \tag{7}$$

The evolution of the damage variables is driven by damage energy release rates:

$$d^{\pm} = f_d(Y^{\pm}), \tag{8}$$

where $f_d(\cdot)$ denotes to a function.

Considering the irreversible deformation during the unloading process, the initial Helmholtz free energies are further decomposed into elastic parts and plastic parts:

$$\Psi_0^{\pm} = \Psi_0^{e\pm} + \Psi_0^{p\pm}. \tag{9}$$

The elastic parts read

$$\Psi_0^{e\pm} = \frac{1}{2}\overline{\boldsymbol{\sigma}}^{\pm} : \boldsymbol{\varepsilon}^e = \frac{1}{2}\overline{\boldsymbol{\sigma}}^{\pm} : (\boldsymbol{\varepsilon} - \boldsymbol{\varepsilon}^p), \tag{10}$$

and the plastic parts read [3]

$$\Psi_0^{p\pm} = \int_0^{\boldsymbol{\varepsilon}^p} \overline{\boldsymbol{\sigma}}^{\pm} : \mathrm{d}\boldsymbol{\varepsilon}^p, \tag{11}$$

where $\boldsymbol{\varepsilon}$, $\boldsymbol{\varepsilon}^e$, and $\boldsymbol{\varepsilon}^p$ are strain tensor, elastic strain tensor and plastic strain tensor, respectively.

Wu et al. [5] adopted the Drucker-Prager plastic model for the compressive plastic Helmholtz free energy Ψ_0^{p-} and neglected the tensile plastic Helmholtz free energy Ψ_0^{p+}. The final expressions for the damage energy release rates are obtained as follows:

$$Y^+ = \sqrt{E_0\left(\overline{\boldsymbol{\sigma}}^+ : \mathbb{C}_0 : \overline{\boldsymbol{\sigma}}\right)}, \tag{12}$$

$$Y^- = \alpha \bar{I}_1 + \sqrt{3\bar{J}_2}, \tag{13}$$

where E_0 is the elastic modulus; $\mathbb{C}_0$ is the compliance tensor; $\bar{I}_1$ is the first invariant of the effective stress tensor; $\bar{J}_2$ is the second invariant of the deviatoric part of the effective stress tensor; and the parameter α is related to the biaxial strength increase, usually $\alpha = 0.12$.

By analogy with the classical plastic theory, the Kuhn-Tucker condition is introduced as the damage evolution criterion:

$$\dot{d}^{\pm} = \dot{\lambda}_d^{\pm} \frac{\partial f_d(Y^{\pm})}{\partial Y^{\pm}}, \quad \dot{\lambda}_d^{\pm} = \dot{r}^{\pm}, \tag{14}$$

$$\begin{cases} \dot{\lambda}_d^{\pm} \geqslant 0, \ F_d(Y^{\pm}, r^{\pm}) = f_d(Y^{\pm}) - f_d(r^{\pm}) \leqslant 0, \\ \dot{\lambda}_d^{\pm} F_d(Y^{\pm}, r^{\pm}) = 0, \end{cases} \tag{15}$$

where $\dot{\lambda}_d^{\pm}$ are damage consistency parameters. The thresholds of damage energy release rates $r^{\pm}$ are given by [3,5]

$$r^{\pm} = \max\left\{r_0^{\pm}, \max_{\tau\in[0,t]} Y_{\tau}^{\pm}\right\}, \tag{16}$$

where $r_0^{\pm}$ are the initial thresholds.

2.2 Plastic strain model

Since the influence of damage is removed from the effective stress space, the plastic strain can be solved by applying the classical plastic theory in the effective stress space.

$$\overline{\boldsymbol{\sigma}} = \mathbb{E}_0 : (\boldsymbol{\varepsilon} - \boldsymbol{\varepsilon}^p), \tag{17}$$

where $\mathbb{E}_0$ is the fourth-order stiffness tensor.

By defining the yield function as F and the plastic potential function as $\tilde{F}$, the plastic strain in effective stress space is solved as [3]

$$\begin{cases} \dot{\boldsymbol{\varepsilon}}^p = \dot{\lambda}_p \dfrac{\partial \tilde{F}(\overline{\boldsymbol{\sigma}}, \boldsymbol{\kappa})}{\partial \overline{\boldsymbol{\sigma}}}, \\ \dot{\kappa} = \dot{\lambda}_p \left[\mathbf{h} \cdot \dfrac{\partial \tilde{F}(\overline{\boldsymbol{\sigma}}, \boldsymbol{\kappa})}{\partial \overline{\boldsymbol{\sigma}}}\right], \\ F(\overline{\boldsymbol{\sigma}}, \boldsymbol{\kappa}) \geqslant 0, \dot{\lambda}_p \leqslant 0, \dot{\lambda}_p F(\overline{\boldsymbol{\sigma}}, \boldsymbol{\kappa}) = 0, \end{cases} \tag{18}$$

where λ_p and $\boldsymbol{\kappa}$ are the plastic flow parameter and the hardening parameter, respectively; $\mathbf{h}$ denotes the vectorial hardening function.

The above effective stress space plasticity provides a rigorous framework for the plastic evolution law. In numerical implementation, assuming the plastic strain increment is proportional to the elastic strain increment for simplicity, a simpler empirical plastic model can be derived as

$$\dot{\boldsymbol{\varepsilon}}^p = H(\dot{d}) f_p(d) \dot{\boldsymbol{\varepsilon}}^e, \tag{19}$$

where $H(\cdot)$ is the Heaviside function and $f_p(\cdot)$ denotes a damage related function.

By fitting experimental data, Ren et al. [19] proposed the form of function $f_p(\cdot)$

$$f_p(d) = \xi_p d^{n_p}, \tag{20}$$

where ξ_p and n_p are fitting parameters.

In the following text, only the compressive plastic strain is considered, and the tensile plastic strain is ignored.

3 Stochastic damage evolution law based on energy dissipation

3.1 Micro-meso stochastic fracture model

In the above deterministic damage framework, the damage evolution function $f_d(\cdot)$ in eq. (8) has to be determined by empirical regression or hypothesis. Moreover, the damage evolution in concrete materials is random in nature, which cannot be reflected in deterministic models. Based on the random medium concept, the MMSF idealizes a representative volume element (RVE) of concrete as a set of parallel microsprings. As shown in Figure 1, the rigid bars at both ends ensure that the strain of each microspring is the same during the loading process. Once the elastic strain of the microspring exceeds the fracture strain, the microspring breaks and damage evolves. By considering the fracture strain of the microspring as a random field, the stochastic damage evolution law can be obtained as [24,25]

$$D = \int_0^1 H(\varepsilon^{e\pm} - \Delta^{\pm}(x))\mathrm{d}x, \tag{21}$$

where $\Delta^{\pm}(x)$ is the random field of fracture strain; $H(\cdot)$ is the Heaviside function; and x denotes the coordinate in the local coordinate system of the microspring.

Usually, $\Delta(x)$ is assumed to be a log-normal distributed

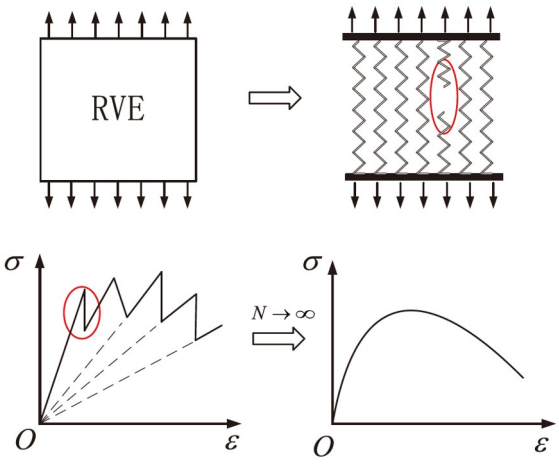

Figure 1 (Color online) Micro-meso stochastic fracture model.

random field and the corresponding normal distributed random field $Z(x) = \ln\Delta(x)$. Assuming the auto-correlation coefficient function of $Z(x)$ is expressed as

$$\rho_Z(y) = \exp(-\omega|y|), \tag{22}$$

where ω is the correlation parameter and $y = x_1 - x_2$ denotes the relative distance between two microsprings.

The mean evolution of the damage variable in eq. (21) can be solved as

$$\mu_D = \Phi_1\left(\frac{\ln\varepsilon^e - \lambda}{\zeta}\right), \tag{23}$$

and the standard deviation is solved as

$$V_D^2 = 2\int_0^1 (1-y)\Phi_2\left(\frac{\ln\varepsilon^e-\lambda}{\zeta}, \frac{\ln\varepsilon^e-\lambda}{\zeta}\middle|\rho_Z(y)\right)\mathrm{d}y - \mu_D^2, \tag{24}$$

where λ and ζ are the mean value and standard deviation of $Z(x)$, respectively; $\Phi_1(\cdot)$ and $\Phi_2(\cdot)$ are the 1D and 2D cumulative probability functions of the standard normal distribution, respectively.

It is worth noting that the above model introduces three model parameters (λ, ζ, and ω) under uniaxial loading, but their values will be different in the case of tension and compression stress states. In the following text, the superscript "+" indicates tension and "–" indicates compression.

In the MMSF, the stress-strain relationship of the microspring is assumed to be the elastic-brittle (Figure 2(a)). Therefore, the stress-strain curves for loading and unloading are identical, proving that there is no energy loss before the microspring breaks. However, studies on the fracture mechanism of the microspring have revealed that multi-scale energy dissipation occurs before its fracture [29,31]. The stress-strain relationship of the microspring may be nonlinear with the energy dissipation process, as shown in Figure 2(b). Hence, the multi-scale energy dissipation within a microspring needs to be studied.

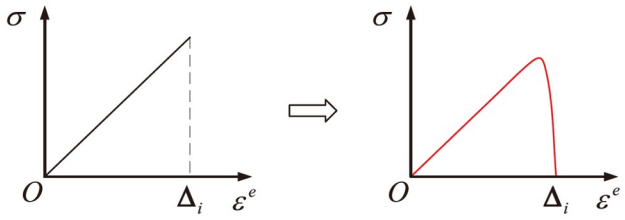

Figure 2 (Color online) Stress-strain relationship of the microspring.

3.2 Energy dissipation of microspring in nanoscale

At the nanoscale, the material particles are connected by the nanoscale adhesion force [32], and the nanocrack tip moves when the external forces exceed the adhesion force. Considering a planner nanocrack that grows in a self-similar manner, the energy dissipation ΔQ caused by crack growth δ_a is expressed as [31]

$$\Delta Q = \delta_a \eta \mathcal{G}_a, \tag{25}$$

where η is the crack geometrical constant and $\mathcal{G}_a$ is the energy release rate in nanoscale.

The atomic arrangements at the crack-tip zone are shown in Figure 3. The circle represents the atoms, and the lines between the atoms represent the interatomic forces. These atoms vibrate at a very high frequency due to thermal activation and the applied load. The vibration makes the atom deviate from its equilibrium position. When the external force is large enough, the distance between the two atoms at the crack tip exceeds the critical state, resulting in the crack growing forward. Therefore, crack propagation can be regarded as a potential energy barrier-crossing process.

The rate-process theory is adopted to dominate the energy barrier-crossing process. Rate process theory describes the behavior of the atomic configuration that results from the random fluctuation of thermal energy. Before the crack grows, the stable atomic configuration keeps the potential energy of the system in the energy valley. For the crack to expand forward, it first needs an external force to provide activation energy of size Q_0 to reach the activated state and cross the energy potential barrier, and then the spatial configuration drops with energy to the next energy valley to keep the system stable. The crack growth rate can be expressed as [31]

$$\dot{a} = \delta_a f, \tag{26}$$

where f is the net energy barrier-crossing rate defined by rate process theory [33].

$$\begin{aligned} f &= \frac{kT}{h}\left[\exp\left(-\frac{Q_0 - \Delta Q/2}{kT}\right) - \exp\left(-\frac{Q_0 + \Delta Q/2}{kT}\right)\right] \\ &= 2\frac{kT}{h}\exp\left(-\frac{Q_0}{kT}\right)\sinh\left(\frac{\Delta Q}{2kT}\right), \end{aligned} \tag{27}$$

where k, h, and T are the Boltzmann constant, Planck con-

stant, and absolute temperature, respectively.

An important assumption of the rate process theory is $\Delta Q \ll kT \ll Q_0$ [31], so eq. (27) can be linearized as

$$f \approx \frac{\Delta Q}{h}\exp\left(-\frac{Q_0}{kT}\right). \tag{28}$$

Assuming a damage increment δ_d that corresponds to the crack growth length δ_a, the damage energy dissipation reads [29]:

$$\Delta Q_d = V_d \int_{d_0}^{d_0+\delta_d} Y \mathrm{d}d, \tag{29}$$

where V_d is the damage volume and d_0 denotes the initial damage state.

The vibration of the nano-particles is at a very high frequency, so the process of bond breaking is very fast. The damage energy release rate during this process can be regarded as a constant. Then eq. (29) becomes

$$\Delta Q_d \approx V_d \delta_d Y. \tag{30}$$

Damage and fracture are two different descriptions of the same physical process, so the energy dissipation should be the same. Hence, we obtain

$$\Delta Q = \delta_a \eta \mathcal{G}_a = \Delta Q_d \approx \delta_d V_d Y. \tag{31}$$

In fact, the number of nanocracks is enormous, and because the shape, initial length, and propagation distances are different among them, the representative values can be taken as a statistical average. The average energy dissipation rate caused by representative nanocrack growth is obtained as

$$\widetilde{\mathcal{G}}_a \dot{\widetilde{a}} = \widetilde{\mathcal{G}}_a \delta_a \frac{\Delta \widetilde{Q}}{h}\exp\left(-\frac{Q_0}{kT}\right). \tag{32}$$

The corresponding energy dissipation in the representative damage volume element reads

$$\widetilde{E}_a = \frac{\int_0^t \widetilde{\mathcal{G}}_a \dot{\widetilde{a}} \mathrm{d}t}{\widetilde{V}_d}, \tag{33}$$

where the superscript "~" denotes the representative value after the statistical average.

3.3 Crack hierarchy model

As shown in Figure 4, the development of material cracks is a multi-level evolutionary process. Initially, the microcracks were scattered randomly at various points. With the increase in loads, new microcracks emerge among the existing microcracks, and some existing microcracks will stop propagating or even close due to stress redistribution. The microcracks continue to propagate and gradually form localized zones. Finally, the localized zone forms larger-scale cracks due to crack coalescence. To bridge the scale gap between the aforesaid energy dissipation process at the nanoscale and the microspring at the microscale, a hierarchy model is introduced here.

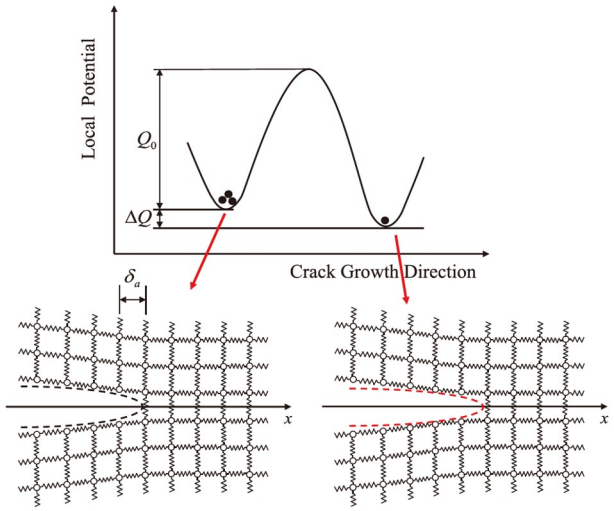

Figure 3 (Color online) Energy barrier denoting crack growth.

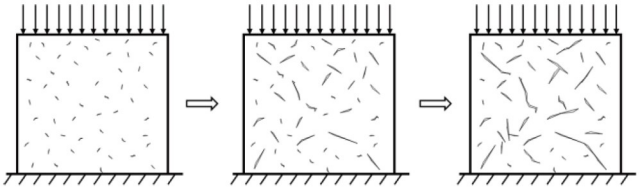

Figure 4 Crack hierarchy model.

Assuming that a representative crack at the larger scale $i+1$ emerges as a result of the propagation and coalescence of n_i cracks at the smaller scale i, then the total number of cracks from the nanoscale to the microscale is given by

$$N = n_1 n_2 \cdots n_s, \tag{34}$$

where s denotes the different scales, from nanoscale to microscale.

The crack number on each scale is a function of the relative crack driving force [31]

$$n_i = g\left(\frac{G}{G_i^c}\right), \tag{35}$$

where G denotes the energy release rate of the microspring and G_i^c denotes the fracture energy at scale i.

By assuming the number of cracks at each scale satisfies self-similarity, the specific expression of function $g(\cdot)$ can be inferred as a power law [29,34]:

$$n_i = \left(\frac{G}{G_i^c}\right)^m. \tag{36}$$

Substituting eq. (36) into eq. (34), the total number of cracks N becomes

$$N = \prod_{i=1}^{s}\left(\frac{G}{G_i^c}\right)^m = \frac{G^{sm}}{\prod_{i=1}^{s}(G_i^c)^m} = \left(\frac{G}{\kappa_c}\right)^p, \tag{37}$$

where $\kappa_c = \prod_{i=1}^{s}\left(G_i^c\right)^{1/s}$ denotes the geometric average of fracture energy from nanoscale to microscale [35]. Considering the inherent randomness of concrete, it can be taken as a random variable.

It is worth noting that although the hierarchical model proposed in this paper is similar to the model proposed by Le et al. [31] in the final expression, the two models are essentially different. In Le's model, it is assumed that the fracture process zone (FPZ) of the crack tip at the larger scale $i+1$ contains n_i cracks at the smaller scale i, and so forth, all the way down to the nanoscale. Obviously, such a model assumes that larger-scale cracks occur before smaller-scale cracks. However, the reality of material failure is that, as illustrated in Figure 4, larger-scale cracks are created by the coalescence and propagation of smaller-scale cracks, which is the key distinction from Le's model.

The energy release rate G in eq. (37) can be replaced by the energy release rate in the context of CDM [36]. Then eq. (37) becomes

$$N = \left(\frac{G}{\kappa_c}\right)^p = \left(\frac{\beta Y}{\kappa_c}\right)^p, \tag{38}$$

where β is a conversion coefficient.

Combining eqs. (33) and (38), the total energy dissipation rate caused by all cracks from nanoscale to microscale is obtained as

$$\begin{aligned}\dot{E}_{\mathrm{mic}} &= N\dot{\widetilde{E}}_a = \frac{\widetilde{\mathcal{G}}_a}{\widetilde{V}_d}\delta_a\frac{\Delta\widetilde{Q}}{h}\exp\left(-\frac{Q_0}{kT}\right)\left(\frac{\beta Y}{\kappa_c}\right)^p \\ &= \frac{\delta_d^2\widetilde{V}_d}{h\eta}\exp\left(-\frac{Q_0}{kT}\right)\left(\frac{\beta Y}{\kappa_c}\right)^p Y^2 \\ &= C\left(\frac{\beta Y}{\kappa_c}\right)^p Y^2 = C_0\left(\frac{Y}{\kappa_c}\right)^p Y^2,\end{aligned} \tag{39}$$

where $C = \frac{\delta_d^2\widetilde{V}_d}{h\eta}\exp\left(-\frac{Q_0}{kT}\right)$ is a model parameter with unit $\mathrm{J}^{-1}\mathrm{m}^3\mathrm{s}^{-1}$ and $C_0 = C\beta^p$.

It is vital to point out that the total energy dissipation rate $\dot{E}_{\mathrm{mic}}$ is within a microspring, and the value of $\dot{E}_{\mathrm{mic}}$ may differ among microsprings of the MMSF. In addition, the expression of $\dot{E}_{\mathrm{mic}}$ is applicable to both tensile and compressive stress states. In the following statement, superscripts "+" and "–" are needed to distinguish two cases.

3.4 Energy dissipation limit of the microspring

Integrating $\dot{E}_{\mathrm{mic}}$ from 0 to time t will give the total energy dissipated during this time period, denoted as E_{mic}. Obviously, the value of E_{mic} cannot be infinite, and therefore a maximum value exists. Here, the elastic fracture energy of the micro-element is adopted as the upper limit. In other words, the cumulative energy dissipation within a microspring should not exceed the elastic fracture energy; otherwise, the microspring will break. As a result, the fracture strain of the microspring can be calculated from this perspective.

In one-dimensional loading cases, the energy release rate Y in eqs. (12) and (13) can be simplified as

$$Y^+ = \overline{\sigma}^+ = E_0\varepsilon^+, \tag{40}$$

$$Y^- = (1-\alpha)\overline{\sigma}^- = (1-\alpha)E_0\varepsilon^{e-}. \tag{41}$$

For uniaxial tension, substituting eq. (40) into eq. (39) and integrating from the start of loading until the microspring breaks, we obtain

$$E_{\mathrm{mic}} = \int_0^t C_0\left(\frac{Y}{\kappa_c}\right)^p Y^2\mathrm{d}t = \int_0^t C_0\frac{(E_0\dot{\varepsilon}t)^{p+2}}{\kappa_c^{\,p}}\mathrm{d}t. \tag{42}$$

The superscript "+" is omitted here. When the strain rate $\dot{\varepsilon}$ is a constant, by changing the integral variable from time to strain, eq. (42) becomes

$$E_{\mathrm{mic}} = \int_0^{\Delta} C_0\frac{(E_0\varepsilon)^{p+2}}{\dot{\varepsilon}\kappa_c^{\,p}}\mathrm{d}\varepsilon = \frac{C_0E_0^{\,p_c+2}\Delta^{\,p_c+3}}{\dot{\varepsilon}\kappa_c^{\,p_c}(p_c+3)}, \tag{43}$$

where Δ is the fracture strain of the microspring, and p_c is the maximum value of p. Since the parameter p now includes the influence of scale number s, this should evolve with the damage parameter. Here, a fixed value p_c is chosen as the representative value for simplicity.

According to the aforementioned energy dissipation threshold, the maximum energy dissipation value during the entire loading process should be equal to the elastic fracture energy. Then we have

$$E_{\mathrm{mic}} = \frac{C_0E_0^{\,p_c+2}\Delta^{\,p_c+3}}{\dot{\varepsilon}\kappa_c^{\,p_c}(p_c+3)} = E_\Delta = \frac{1}{2}E_0\Delta^2. \tag{44}$$

Thus, the tensile fracture strain can be derived as

$$\Delta = \left[\frac{(p_c+3)\dot{\varepsilon}}{2C_0E_0^{\,p_c+1}}\kappa_c^{\,p_c}\right]^{\frac{1}{p_c+1}}. \tag{45}$$

For uniaxial compression, by substituting eq. (41) into eq. (39) and integrating the whole elastic energy dissipation process, we can also obtain the expression of E_{mic} as follows:

$$E_{\mathrm{mic}} = \frac{C_0[(1-\alpha)E_0]^{p_c+2}\Delta^{\,p_c+3}}{\dot{\varepsilon}^e\kappa_c^{\,p_c}(p_c+3)}, \tag{46}$$

where $\dot{\varepsilon}^e$ denotes the elastic strain rate.

Therefore, the shear fracture strain can be derived as

$$\Delta = \left[\frac{(p_c+3)\dot{\varepsilon}^e}{2C_0((1-\alpha)E_0)^{p_c+1}}\kappa_c^{\,p_c}\right]^{\frac{1}{p_c+1}}. \tag{47}$$

3.5 Damage evolution law of RVE

By changing the fracture strain in the damage evolution expression to energy dissipation, the new damage evolution

law becomes

$$\begin{cases} D=\int_0^1 H(E_{\mathrm{mic}}-E_{\Delta})\mathrm{d}x, \\ E_{\Delta}=\dfrac{1}{2}E_0\Delta^2(x). \end{cases} \tag{48}$$

By introducing eq. (45), the final expression for the tensile stochastic damage evolution law is written as

$$\begin{cases} D=\int_0^1 H(E_{\mathrm{mic}}-E_{\Delta})\mathrm{d}x, \\ E_{\mathrm{mic}}=\int_0^t C_0\left(\dfrac{Y}{\kappa_c}\right)^{p_c}Y^2\mathrm{d}t, \\ E_{\Delta}=\dfrac{1}{2}E_0\left[\dfrac{(p+3)\dot{\varepsilon}}{2C_0E_0{}^{p_c+1}}\kappa_c{}^{p_c}\right]^{\frac{2}{p_c+1}}. \end{cases} \tag{49}$$

Similarly, the shear stochastic damage evolution law can be obtained as follows:

$$\begin{cases} D=\int_0^1 H(E_{\mathrm{mic}}-E_{\Delta})\mathrm{d}x, \\ E_{\mathrm{mic}}=\int_0^t C_0\left(\dfrac{Y}{\kappa_c}\right)^{p_c}Y^2\mathrm{d}t, \\ E_{\Delta}=\dfrac{1}{2}E_0\left\{\dfrac{(p+3)\varepsilon^e}{2C_0[(1-\alpha)E_0]^{p_c+1}}\kappa_c{}^{p_c}\right\}^{\frac{2}{p_c+1}}. \end{cases} \tag{50}$$

Different from Ding's work [29], the fracture strain is given from the perspective of energy dissipation, and it is not necessary to consider fatigue damage energy dissipation and monotonic damage energy dissipation separately. Besides, Wang and Li [35] also examined the microspring's energy dissipation process, but they failed to determine the fracture strain that corresponds to the energy dissipation limit. In this work, eqs. (45) and (47) essentially establish the connection between fracture strain $\Delta(x)$ and nano-micro comprehensive fracture energy κ_c.

From this perspective, an alternative expression of the stochastic damage evolution law can be given. Substituting eq. (45) into eq. (39) and eliminating κ_c, we obtain the new expression for $\dot{E}_{\mathrm{mic}}$:

$$\dot{E}_{\mathrm{mic}}=\frac{\dot{\varepsilon}(p_c+3)Y^{p_c+2}}{2E_0{}^{p_c+1}\Delta^{p_c+1}}. \tag{51}$$

Then the tensile stochastic damage evolution law in eq. (49) becomes

$$\begin{cases} D=\int_0^1 H(E_{\mathrm{mic}}-E_{\Delta})\mathrm{d}x, \\ E_{\mathrm{mic}}=\int_0^t \dfrac{\dot{\varepsilon}(p_c+3)Y^{p_c+2}}{2E_0{}^{p_c+1}\Delta^{p_c+1}}\mathrm{d}t, \\ E_{\Delta}=\dfrac{1}{2}E_0\Delta^2. \end{cases} \tag{52}$$

Likewise, the alternate expression for the shear stochastic damage evolution law is written as

$$\begin{cases} D=\int_0^1 H(E_{\mathrm{mic}}-E_{\Delta})\mathrm{d}x, \\ E_{\mathrm{mic}}=\int_0^t \dfrac{\dot{\varepsilon}^e(p_c+3)Y^{p_c+2}}{2[(1-\alpha)E_0]^{p_c+1}\Delta^{p_c+1}}\mathrm{d}t, \\ E_{\Delta}=\dfrac{1}{2}E_0\Delta^2. \end{cases} \tag{53}$$

In contrast to eq. (21), eqs. (52) and (53) essentially provide a fracture process for the microspring.

The nonlinear constitutive law of the microspring can be derived if the dissipated energy is interpreted as some sort of microdamage to the microspring.

$$\sigma=(1-d_{\mathrm{micro}})E_0\varepsilon^e, \tag{54}$$

where the rate of the microdamage $\dot{d}_{\mathrm{micro}}$ is expressed as

$$\dot{d}_{\mathrm{micro}}=\frac{\dot{E}_{\mathrm{mic}}}{E_{\Delta}}. \tag{55}$$

For uniaxial tension, eq. (55) becomes

$$\dot{d}_{\mathrm{micro}}=\frac{\dot{\varepsilon}(p_c+3)}{\Delta}\left(\frac{\varepsilon}{\Delta}\right)^{p_c+2}. \tag{56}$$

Similarly, the microdamage rate for uniaxial compression is obtained as follows:

$$\dot{d}_{\mathrm{micro}}=\frac{\dot{\varepsilon}^e(p_c+3)(1-\alpha)}{\Delta}\left(\frac{\varepsilon^e}{\Delta}\right)^{p_c+2}. \tag{57}$$

3.6 Rate-dependent extension

The mechanical behavior of concrete materials is well recognized as being sensitive to strain rate. Dynamic loads such as impacts and earthquakes will cause a higher strain rate in engineering structures. The proposed model is not intended to provide a substitute for the original micro-meso stochastic fracture model but to provide a unified framework for other loading cases. Since the derivations in eqs. (42) and (43) are valid for different loading rates, the rate-dependent model can be established by deriving the fracture strain under different loading rates.

According to eq. (45) or eq. (47), the dynamic fracture strain is expressed as

$$\frac{\Delta_d}{\Delta_s}=\frac{E_{0,s}}{E_{0,d}}\left(\frac{\dot{\varepsilon}_d}{\dot{\varepsilon}_s}\right)^{\frac{1}{p_c+1}}\left(\frac{\kappa_{c,d}}{\kappa_{c,s}}\right)^{\frac{p_c}{p_c+1}}, \tag{58}$$

where the subscripts d and s represent dynamic and static properties, respectively.

Eq. (58) demonstrates that the strain rate, dynamic elastic modulus, and dynamic fracture energy are the three components that define the dynamic fracture strain.

4 Parameter analysis

In addition to the three parameters in the original MMSF,

which can be identified by the least-squares criterion, a new parameter, p_c, is introduced in the proposed model. The parameter analysis is given here.

Monotonic loading with a strain rate of 1×10^{-5}/s is considered here. A numerical sample including 1000 discrete microsprings is given based on the stochastic harmonic function method [37]. For ease of analysis, the microsprings in the sample are arranged in ascending order of fracture strain. The elastic modulus E_0=3.5×10^4 N/mm^2. The three parameters characterizing the tensile fracture strain for C50 concrete were provided by Zeng [38] through inverse identification with 132 experimental stress-strain data: $\lambda^+ = 4.8696$, $\zeta^+ = 0.5828$ and $\omega^+ = 62$.

Figure 5(a) gives the same monotonic stress-strain curves with different p_c^+ values. It seems that the curves are insensitive to p_c^+. Because under monotonic loading cases, the damage evolution law in eq. (52) only concerns whether the maximum value of E_{mic} exceeds E_Δ, not the evolution process of E_{mic}. However, if we take into account other loading types, including cyclic loading, the evolution of E_{mic} becomes crucial. The energy dissipation process of a typical microspring is plotted in Figure 5(b) with different p_c^+. Obviously, it has an influence on the evolution process of E_{mic}, which plays a key role in cyclic loading.

In fact, the energy dissipation process can be roughly divided into two stages. The first stage consumes a very small amount of energy. It moves to the second stage when the external load reaches a certain level. Energy dissipation starts to rise tremendously. As p_c^+ increases, the energy dissipation of the first stage decreases relatively, but the second stage rises faster in order to reach the same fracture point. Figure 5(c) depicts the microdamage evolution of a typical microspring, which exhibits the same characteristics as energy dissipation. Therefore, the stress-strain curve of the microspring is approximately linear in the first stage, and as the microdamage evolves, the stress eventually declines to zero (Figure 5(d)). With increasing p_c^+, the microspring's constitutive law tends to resemble the linear elastic constitutive law assumed by the original model. In other words, the original model can be seen as a linearization of the proposed model.

Additionally, after gaining the dynamic properties of concrete, the impact of parameter p_c^+ on the dynamic increase factor (DIF) of strength is investigated, and the results are depicted in Figure 6. The quasi-static strain rate is set to 1×10^{-5}/s. It is found that p_c^+ governs the rising speed of DIF; hence, the relevant experimental data can be used to identify the parameter p_c^+. In the following analysis, $p_c^+ = 20$ and $p_c^- = 25$ are adopted in the numerical calculation.

5 Model verification

5.1 Uniaxial tension

As mentioned before, the stochastic damage evolution laws defined by eqs. (21) and (52) are identical. The above-

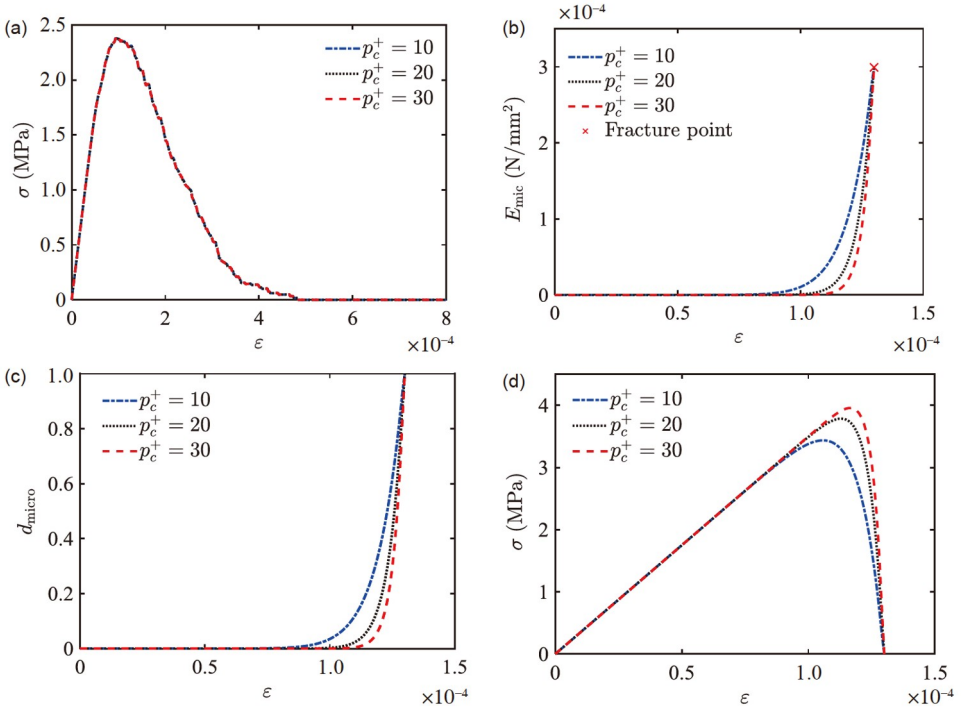

Figure 5 (Color online) (a) Stress-strain of the RVE; (b) energy dissipation process of a typical microspring; (c) microdamage evolution of a typical microspring; (d) stress-strain curve of a typical microspring.

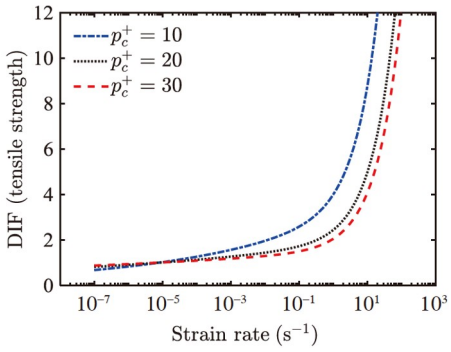

Figure 6 (Color online) Influence of parameter p_c on strength DIF.

mentioned numerical tension sample is presented here for verification. With a strain rate of 1×10^{-5}/s and $p_c^+ = 20$, the stress-strain curve and damage evolution of this sample are shown in Figure 7(a) and (b). The results calculated by eqs. (21) and (52) are displayed in the legend as MMSF-Δ and MMSF-E_{mic}, respectively. It can be found that, for monotonic loading, the two damage evolution laws give the same results.

Despite the two formulas' consistency in damage evolution at the RVE level, the latter can provide more details on the microdamage process of the microspring. In Figure 8(a), the energy dissipation processes of all microsprings are presented. All the microsprings' energy dissipation processes are actually similar under monotonic loading, only with different fracture strains. Based on the previously defined microdamage, the stress-strain curves for three microsprings with fracture strains at 4.9×10^{-5}, 1.3×10^{-4}, and 2.6×10^{-4}, respectively, are depicted in Figure 8(b)–(d). Obviously, the stress-strain relationship is no longer elastic-brittle as assumed previously but has nonlinear properties with the development of microdamage. The tensile strength of this sample is around 2.4 MPa; some microsprings with small fracture strains will break before reaching the tensile strength (Figure 8(b)). In contrast, those microsprings with greater fracture strains will bear greater stress due to stress redistribution, as shown in Figure 8(c) and (d).

5.2 Uniaxial compression

The parameters defining shear fracture strains for C50 concrete are identified as $\lambda^- = 7.5668$, $\zeta^- = 0.2546$ and $\omega^- = 84$ [38]. The stochastic harmonic function method is also employed to provide a numerical sample with 1000 discrete microsprings. The plastic model parameters in the example are set as follows: $\xi_p = 2.5$, $n_p = 0.2$. With strain rate $\dot{\varepsilon} = 1\times10^{-5}$/s, Figure 9 displays the damage evolution curves and the stress-strain curves. MMSF-Δ and MMSF-E_{mic} in the legend stand for the damage evolution law defined by eqs. (21) and (53). It is proven that the results of the two methods are consistent under monotonic loading. Since plastic strain is taken into account in monotonic compressive loading, each incremental step requires a modification to the elastic strain rate.

Figure 10(a) illustrates how the strain and its components in this sample develop as loading time increases. It can be seen that the elastic strain dominates at the beginning of the loading process, while the plastic strain takes over as the loading progresses. In Figure 10(b) [39–41], the shifting trend of plastic strain is in good agreement with the experimental data. ε_c in Figure 10(b) denotes the strain corresponding to the peak stress. It is proven that the empirical plastic model in eq. (19) can well describe the irreversible deformation of concrete during compression.

Figure 11(a) shows the energy dissipation processes for all the microsprings. According to the energy dissipation process, the related microdamage can be obtained. Three typical microsprings with different fracture strains are selected to draw the corresponding stress-strain curves in Figure 11(b)–(d). The main mechanical behavior of the microspring is consistent with uniaxial tension. However, it is important to note that elastic deformation engages in the above-defined energy dissipation whereas plastic deformation does not; hence, the horizontal coordinates in Figure 11 indicate the elastic strain.

5.3 Rate dependent examples

The proposed model can be employed in dynamic loading

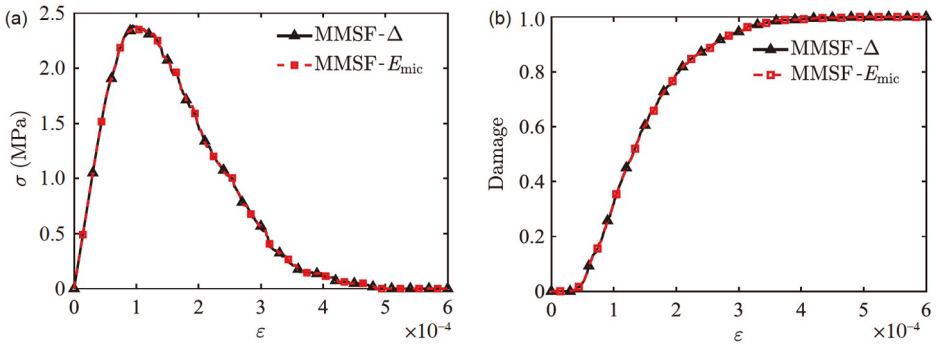

Figure 7 (Color online) (a) Stress-strain curve; (b) damage evolution.

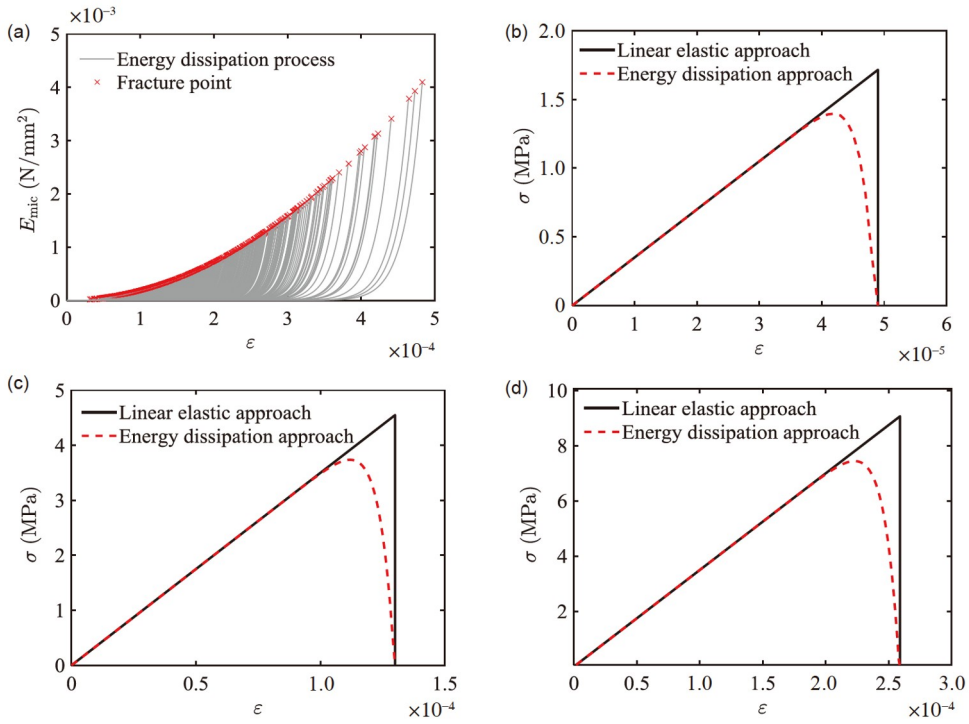

Figure 8 (Color online) (a) Energy dissipation process of all microsprings; (b) stress-strain curve of 30th microspring; (c) stress-strain curve of 500th microspring; (d) stress-strain curve of 900th microspring.

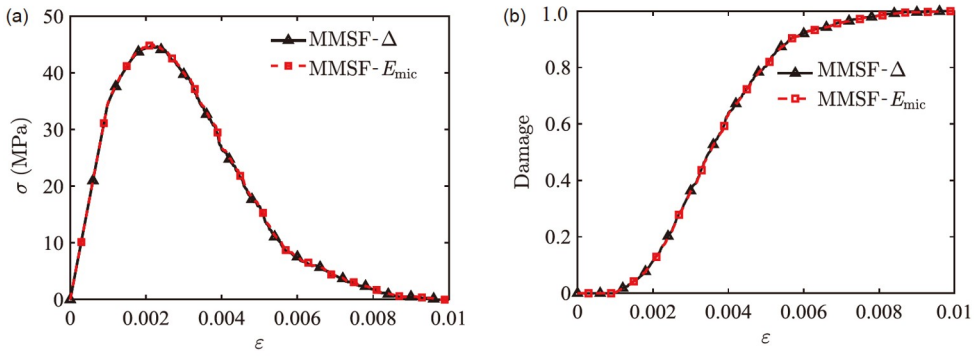

Figure 9 (Color online) (a) Stress-strain curve; (b) damage evolution.

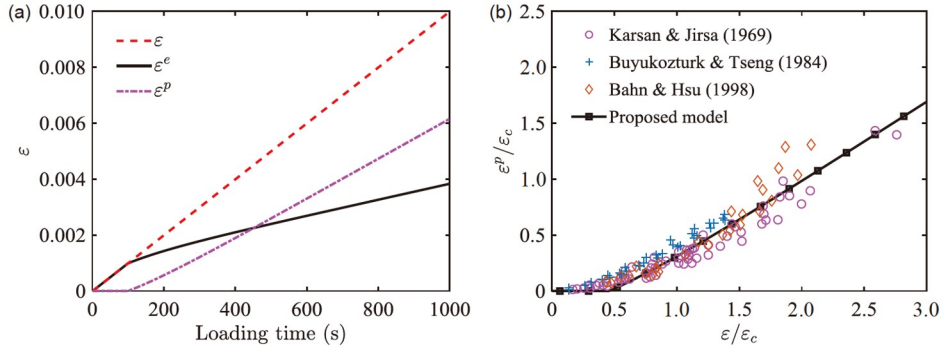

Figure 10 (Color online) (a) Variation of strain and its components; (b) empirical plastic model.

cases, while the original model is only suitable for static ones. According to eq. (58), the fracture strain of the microspring increases with the increase in strain rate, which leads to an increase in material strength. As stated by eq. (58), the dynamic fracture strain is determined by the dynamic mechanical properties of concrete. Hence, it is essential to ascertain how the strain rate affects the dynamic mechanical properties of concrete. As illustrated in Figure 12 [42–45], test data fitting yields dynamic properties such as dynamic elastic modulus and dynamic fracture energy.

The fitting curve is a power-law type that reads

$$\mathrm{DIF} = a\left(\dot{\varepsilon}^{b} - \dot{\varepsilon}_{s}^{b}\right) + 1, \tag{59}$$

where a and b are fitting parameters, and the static strain rate $\dot{\varepsilon}_{s}=1\times10^{-5}$/s.

The static tensile fracture energy $\kappa_{c,s}$=150 N/m yields a_1=0.4159 and b_1=0.6023. However, due to a lack of test data, it is questionable how the shear fracture energy would vary as the strain rate increased. In the following analysis, the shear fracture energy parameters are inversely identified using the DIF of compression strength, yielding the values a_2=0.0025 and b_2=0.8029. The parameters for dynamic elastic modulus are identical for both tension and shear mechanisms, yielding a_3=0.5808 and b_3=0.1435.

Numerical simulations under uniaxial loading cases are performed here. For uniaxial tension, 50 C50 samples are used to calculate the stress-strain curve for each of the three strain rates: $\dot{\varepsilon}_1=1\times10^{-5}$/s, $\dot{\varepsilon}_2=1\times10^{-4}$/s, and $\dot{\varepsilon}_3=1\times10^{-2}$/s. The simulated results are displayed in Figure 13 along with the experimental data. Model-Mean and Model-Std in the

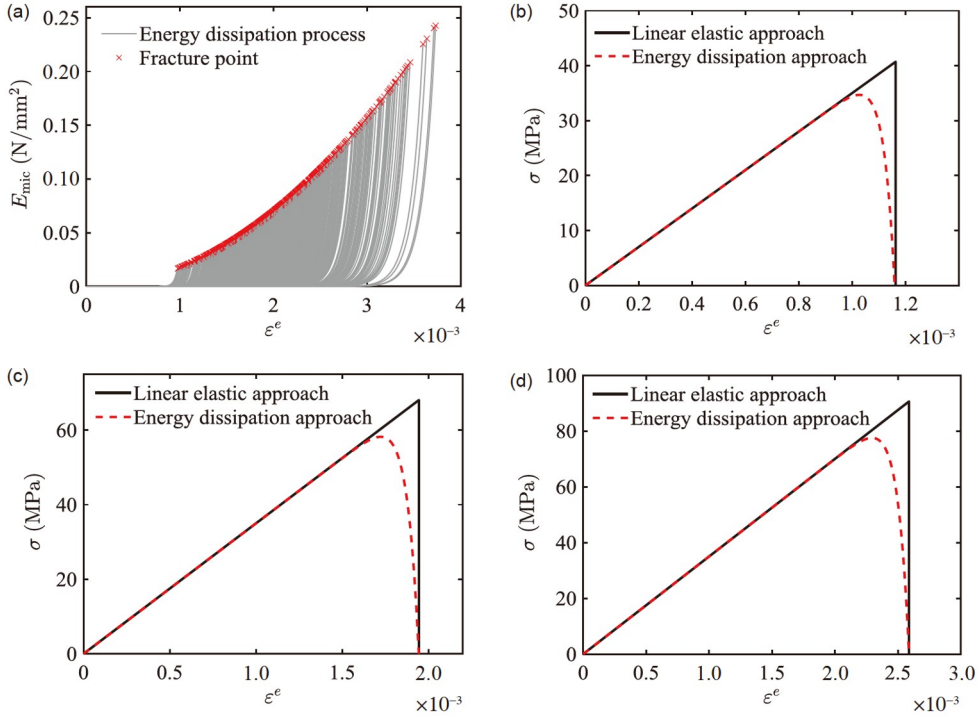

Figure 11 (Color online) (a) Energy dissipation process of all springs; (b) stress-strain curve of 30th microspring; (c) stress-strain curve of 500th microspring; (d) stress-strain curve of 900th microspring.

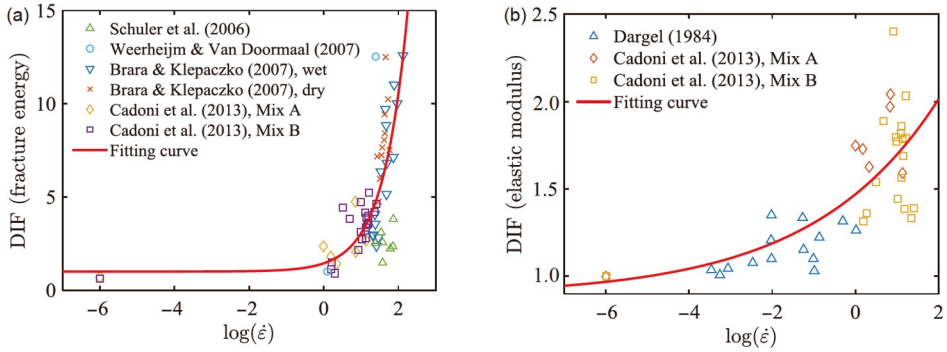

Figure 12 (Color online) Dynamic properties of concrete. (a) Tensile fracture energy; (b) elastic modulus.

legend stand for the mean and standard deviation of the stress-strain curve calculated by the proposed model. Exp-Mean and Exp-Std denote the mean and standard deviation of the experimental data. The experimental data were gathered from Gao et al. [46]. As can be observed, the experimental data and model results for various strain rates agree well.

A sample is selected for detailed analysis. Figure 14(a) depicts the stress-strain relationship of this sample. Due to the fact that the fracture strain of the microspring is larger at a higher strain rate, the tensile strength increases as the strain rate increases. Figure 14(b)–(d) illustrate a typical microspring's energy dissipation process, microdamage evolution, and stress-strain relationship, respectively. It is found that the mechanical properties of the microspring change accordingly with the strain rate.

Likewise, 50 samples are generated for uniaxial compression using the stochastic harmonic function approach. Figure 15 presents the stress-strain curves under three different strain rates. The experiment data were collected from Zeng [38]. As can be observed, the stress-strain curve's mean value and standard deviation predicted by the proposed model agree with the experimental results under various strain rates.

A specific sample is chosen to gain more detailed information. The stress-strain curves in Figure 16(a) demonstrate that the proposed model can accurately capture the increase in compressive strength under dynamic load. The

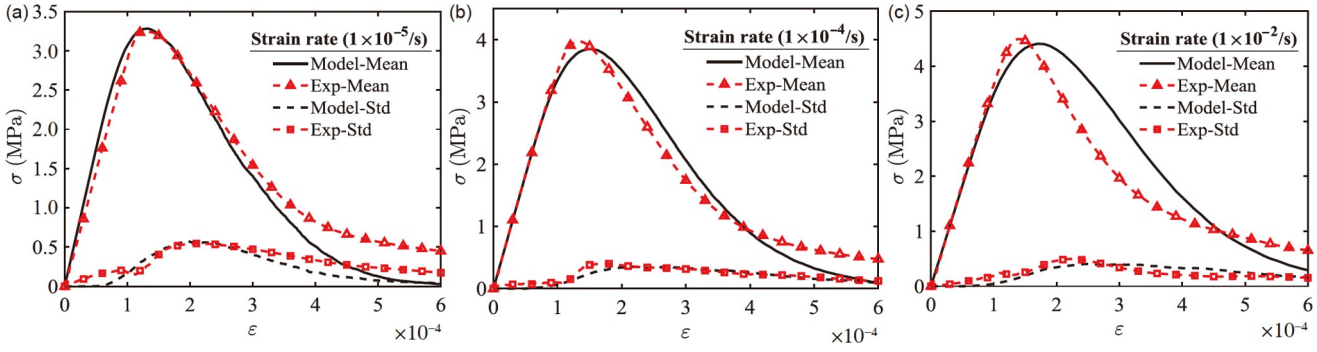

Figure 13 (Color online) Stress-strain curves for various strain rates under uniaxial tension. (a) $\dot{\varepsilon}_1=1\times10^{-5}$/s; (b) $\dot{\varepsilon}_2=1\times10^{-4}$/s; (c) $\dot{\varepsilon}_3=1\times10^{-2}$/s.

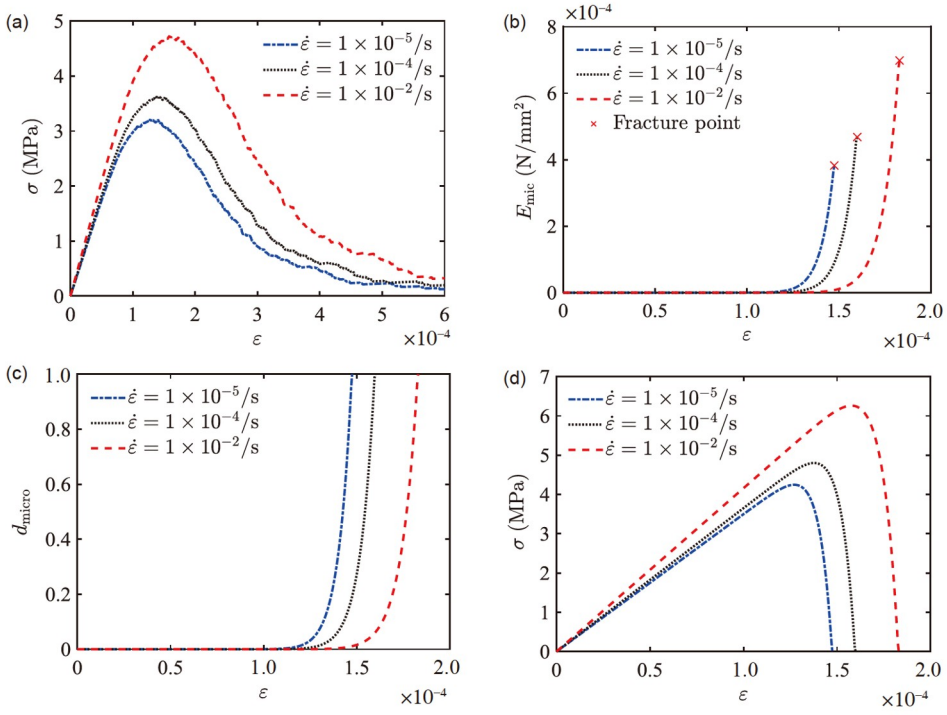

Figure 14 (Color online) (a) Stress-strain of a typical sample; (b) energy dissipation process of a typical microspring; (c) microdamage evolution of a typical microspring; (d) stress-strain curve of a typical microspring.

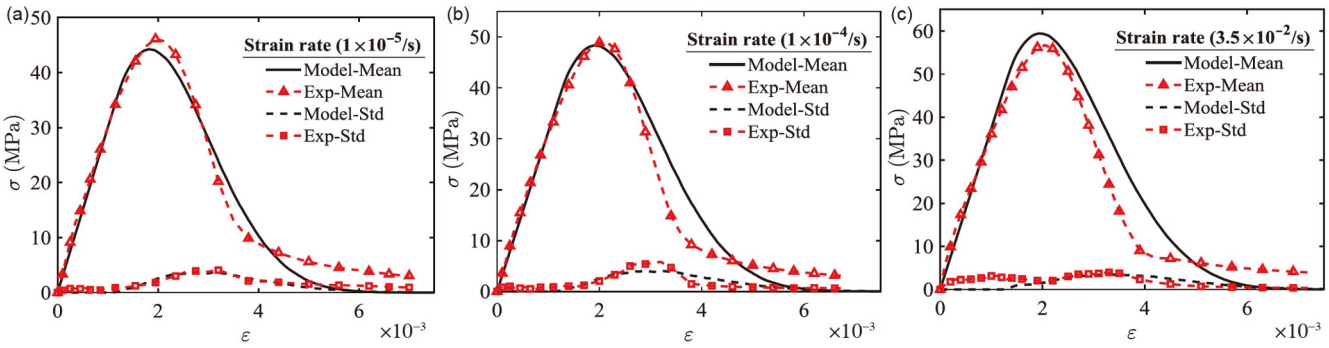

Figure 15 (Color online) Stress-strain curves for various strain rates under uniaxial compression. (a) $\dot{\varepsilon}_1 = 1\times10^{-5}$/s; (b) $\dot{\varepsilon}_2 = 1\times10^{-4}$/s; (c) $\dot{\varepsilon}_3 = 3.5\times10^{-2}$/s.

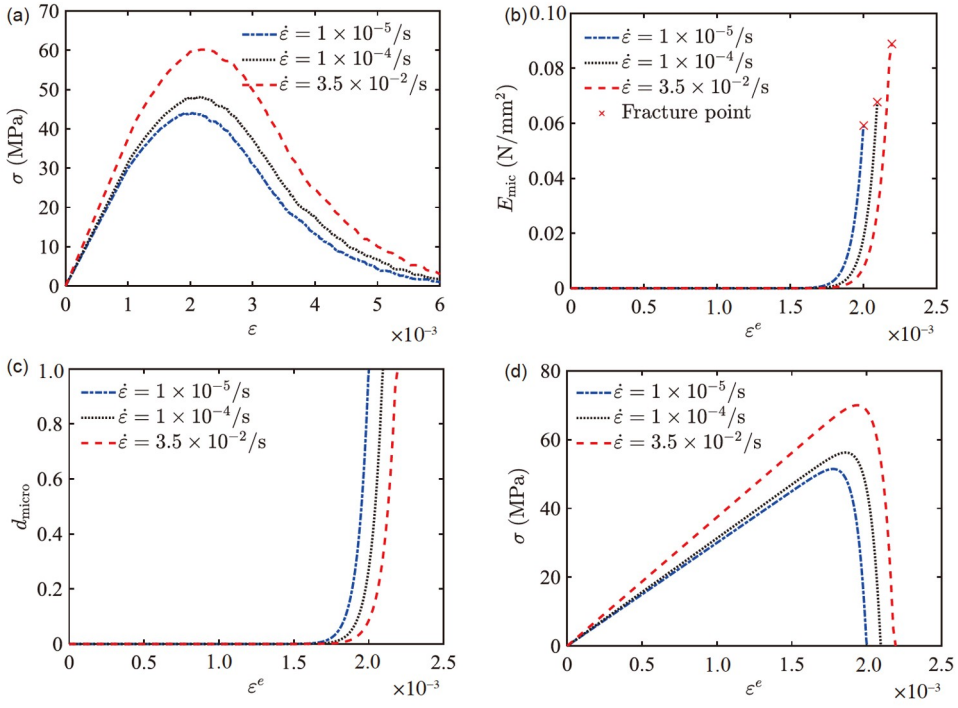

Figure 16 (Color online) (a) Stress-strain of a typical sample; (b) energy dissipation process of a typical microspring; (c) microdamage evolution of a typical microspring; (d) stress-strain curve of a typical microspring.

energy dissipation process of a typical microspring in Figure 16(b) verifies that the higher strain rate leads to a larger fracture strain, which allows the microdamage evolution of the microspring to delay (Figure 16(c)). Therefore, the strength of the microspring increases at a higher strain rate (Figure 16(d)).

The DIF of the strength is investigated and contrasted with the experimental data in order to clarify the scope of application. For each strain rate, 20 samples are calculated, and the quasi-static rate is set at 1×10^{-5}/s. The results are shown in Figure 17 [47–58]. At strain rates ranging from 1×10^{-7}/s to 1×10^{2}/s, it is found that the model results and the experimental data are in good agreement.

6 Conclusions

A unified damage model is proposed in this work by taking into account the multi-scale energy dissipation process of the microspring in the micro-meso stochastic model. The crack growth velocity is described using rate process theory at the nanoscale within one microspring. The crack hierarchy model is then employed to determine the crack number from the nanoscale to the microscale. Consequently, the stochastic damage evolution law is expressed by the energy dissipation threshold instead of fracture strain. The proposed model can be extended to include rate dependence by identifying fracture strains at different strain rates. Numerical examples are

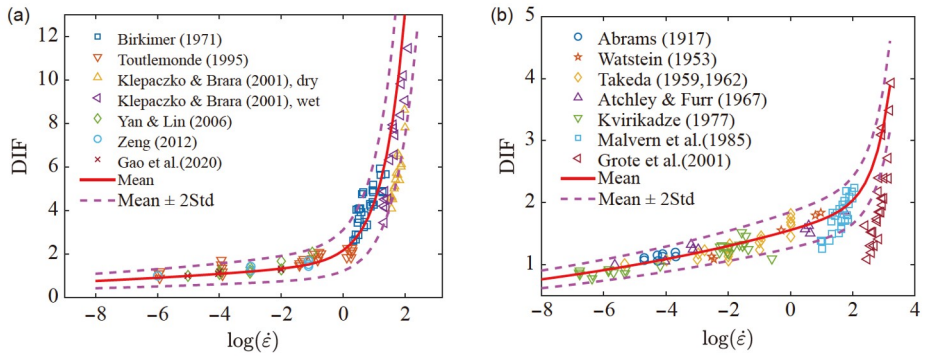

Figure 17 (Color online) (a) DIF under tension; (b) DIF under compression.

provided to demonstrate the effectiveness of the proposed model. Several concluding remarks could be summarized as follows.

(1) Using the elastic strain energy as an upper bound and incorporating the energy dissipation process, the fracture strain of the microspring in the MMSF can be derived.

(2) With the help of the derived fracture strain, the damage evolution law based on the energy dissipation threshold is consistent with the damage evolution law based on fracture strain in the original MMSF.

(3) The model can be extended to rate-dependent cases by deriving the dynamic fracture strain according to the dynamic properties of concrete.

(4) The proposed model can take into account the microdamage prior to fracture of the microspring, laying the foundation for extending the model to fatigue loading cases.

This work was supported by the National Natural Science Foundation of China (Grant No. 51538010).

1 Mazars J. A description of micro-and macroscale damage of concrete structures. Eng Fracture Mech 1986, 25: 729–737
2 Simo J C, Ju J W. Strain- and stress-based continuum damage models—I. Formulation. Int J Solids Struct, 1987, 23: 821–840
3 Ju J W. On energy-based coupled elastoplastic damage theories: Constitutive modeling and computational aspects. Int J Solids Struct, 1989, 25: 803–833
4 Faria R, Oliver J, Cervera M. A strain-based plastic viscous-damage model for massive concrete structures. Int J Solids Struct, 1998, 35: 1533–1558
5 Wu J Y, Li J, Faria R. An energy release rate-based plastic-damage model for concrete. Int J Solids Struct, 2006, 43: 583–612
6 Barchiesi E, Misra A, Placidi L, et al. Granular micromechanics-based identification of isotropic strain gradient parameters for elastic geometrically nonlinear deformations. Z Angew Math Mech, 2021, 101: e202100059
7 Timofeev D, Barchiesi E, Misra A, et al. Hemivariational continuum approach for granular solids with damage-induced anisotropy evolution. Math Mech Solids, 2021, 26: 738–770
8 Placidi L, Barchiesi E, Misra A, et al. Micromechanics-based elasto-plastic-damage energy formulation for strain gradient solids with granular microstructure. Continuum Mech Thermodyn, 2021, 33: 2213–2241
9 Bischoff P H, Perry S H. Compressive behaviour of concrete at high strain rates. Mater Struct, 1991, 24: 425–450
10 Brara A, Klepaczko J R. Fracture energy of concrete at high loading rates in tension. Int J Impact Eng, 2007, 34: 424–435
11 Ožbolt J, Sharma A, İrhan B ı, et al. Tensile behavior of concrete under high loading rates. Int J Impact Eng, 2014, 69: 55–68
12 Feng Y, Fan J, Tadmor E B. A rigorous universal model for the dynamic strength of materials across loading rates. J Mech Phys Solids, 2022, 159: 104715
13 Rossi P. A physical phenomenon which can explain the mechanical behaviour of concrete under high strain rates. Mater Struct, 1991, 24: 422–424
14 Cadoni E, Labibes K, Albertini C, et al. Strain-rate effect on the tensile behaviour of concrete at different relative humidity levels. Mat Struct, 2001, 34: 21–26
15 Reinhardt H W, Weerheijm J. Tensile fracture of concrete at high loading rates taking account of inertia and crack velocity effects. Int J Fract, 1991, 51: 31–42
16 Brara A, Klepaczko J R. Experimental characterization of concrete in dynamic tension. Mech Mater, 2006, 38: 253–267
17 Cervera M, Oliver J, Manzoli O. A rate-dependent isotropic damage model for the seismic analysis of concrete dams. Earthquake Engng Struct Dyn, 1996, 25: 987–1010
18 Dubé J F, Pijaudier-Cabot G, Borderie C L. Rate dependent damage model for concrete in dynamics. J Eng Mech, 1996, 122: 939–947
19 Ren X, Zeng S, Li J. A rate-dependent stochastic damage-plasticity model for quasi-brittle materials. Comput Mech, 2015, 55: 267–285
20 Cusatis G. Strain-rate effects on concrete behavior. Int J Impact Eng, 2011, 38: 162–170
21 Hai L, Wu J Y, Li J. A phase-field damage model with micro inertia effect for the dynamic fracture of quasi-brittle solids. Eng Fract Mech, 2020, 225: 106821
22 Krajcinovic D, Silva M A G. Statistical aspects of the continuous damage theory. Int J Solids Struct, 1982, 18: 551–562
23 Kandarpa S, Kirkner D J, Spencer Jr. B F. Stochastic damage model for brittle materials subjected to monotonic loading. J Eng Mech, 1996, 122: 788–795
24 Li J, Zhang Q Y. Study of stochastic damage constitutive relationship for concrete material (in Chinese). J Tongji Univ Nat Sci, 2001, 29: 1135–1141
25 Li J, Ren X. Stochastic damage model for concrete based on energy equivalent strain. Int J Solids Struct, 2009, 46: 2407–2419
26 Liang S X, Ren X D, Li J. A random medium model for simulation of concrete failure. Sci China Tech Sci, 2013, 56: 1273–1281
27 Li J, Wu J Y, Chen J B. Stochastic Damage Mechanics of Concrete Structures (in Chinese). Beijing: Science Press, 2014
28 Liu H, Ren X, Li J. Indentation tests based multi-scale random media modeling of concrete. Construct Build Mater, 2018, 168: 209–220
29 Ding Z, Li J. A physically motivated model for fatigue damage of concrete. Int J Damage Mech, 2018, 27: 1192–1212

30 Lemaitre J. Evaluation of dissipation and damage in metals submitted to dynamic loading. In: Proceedings of the International Conference on Mechanical Behavior of Materials. Kyoto, 1971
31 Le J L, Bažant Z P, Bazant M Z. Unified nano-mechanics based probabilistic theory of quasibrittle and brittle structures: I. Strength, static crack growth, lifetime and scaling. J Mech Phys Solids, 2011, 59: 1291–1321
32 Rivas Murillo J S, Mohamed A, Hodo W, et al. Computational modeling of shear deformation and failure of nanoscale hydrated calcium silicate hydrate in cement paste: Calcium silicate hydrate Jennite. Int J Damage Mech, 2016, 25: 98–114
33 Hänggi P, Talkner P, Borkovec M. Reaction-rate theory: Fifty years after Kramers. Rev Mod Phys, 1990, 62: 251–341
34 Barenblatt G I, Barenblatt G I, Isaakovich B G. Scaling, Self-Similarity, and Intermediate Asymptotics: Dimensional Analysis and Intermediate Asymptotics. Cambridge: Cambridge University Press, 1996
35 Wang Y, Li J. A two-scale stochastic damage model for concrete under fatigue loading. Int J Fatigue, 2021, 153: 106508
36 Mazars J, Pijaudier-Cabot G. From damage to fracture mechanics and conversely: A combined approach. Int J Solids Struct, 1996, 33: 3327–3342
37 Chen J, Sun W, Li J, et al. Stochastic harmonic function representation of stochastic processes. J Appl Mech, 2013, 80: 011001
38 Zeng S J. Dynamic experimental research and stochastic damage constitutive model for concrete (in Chinese). Dissertation for Doctoral Degree. Shanghai: Tongji University, 2012
39 Karsan I D, Jirsa J O. Behavior of concrete under compressive loadings. J Struct Div, 1969, 95: 2543–2564
40 Buyukozturk O, Tseng T. Concrete in biaxial cyclic compression. J Struct Eng, 1984, 110: 461–476
41 Bahn B Y, Hsu C T T. Stress-strain behavior of concrete under cyclic loading. ACI Mater J, 1998, 95: 178–193
42 Schuler H, Mayrhofer C, Thoma K. Spall experiments for the measurement of the tensile strength and fracture energy of concrete at high strain rates. Int J Impact Eng, 2006, 32: 1635–1650
43 Weerheijm J, Van Doormaal J C A M. Tensile failure of concrete at high loading rates: New test data on strength and fracture energy from instrumented spalling tests. Int J Impact Eng, 2007, 34: 609–626
44 Cadoni E, Solomos G, Albertini C. Concrete behaviour in direct tension tests at high strain rates. Mag Concrete Res, 2013, 65: 660–672
45 Dargel H J. Zur rechnerischen analyse von stahlbetontragwerken unter stossartiger beanspruchung (In German). Dissertation for Doctoral Degree. Darmstadt: Darmstadt University, 1984
46 Gao X, Zhou L, Ren X, et al. Rate effect on the stress-strain behavior of concrete under uniaxial tensile stress. Struct Concrete, 2021, 22: E815
47 Birkimer D L, Lindemann R. Dynamic tensile strength of concrete materials. J Proc, 1971, 68: 47–49
48 Toutlemonde F. Impact resistance of concrete structures (In French). Dissertation for Doctoral Degree. Paris: Ecole Nationale des Ponts et Chaussées, Laboratory of Bridges and Roads, 1995
49 Klepaczko J R, Brara A. An experimental method for dynamic tensile testing of concrete by spalling. Int J Impact Eng, 2001, 25: 387–409
50 Yan D, Lin G. Dynamic properties of concrete in direct tension. Cement Concrete Res, 2006, 36: 1371–1378
51 Abrams D A. Effect of rate of application of load on the compressive strength of concrete. Proc ASTM, 1917, 17: 364–377
52 Watstein D. Study of stochastic damage constitutive relationship for concrete material. J Proc, 1953, 49: 729–744
53 Takeda J. A Loading apparatus for high speed testing of building materials and structiutes. In: Proceedings of the 2nd Japan Congress on Testing Materials. Kyoto, 1959
54 Takeda J. The mechanical properties of several kinds of concretes at compressive, tensile and flexural tests in high rates of loading. Transactions of the Architectural Institute of Japan, 1962, 77: 1–6
55 Atchley B L, Furr H L. Strength and energy absorption capablities of plain concrete under dynamic and static loadings. J Proc, 1967, 64: 745–756
56 Kvirikadze O P. Determination of the ultimate strength and modulus of deformation of concrete at different rates of loading. In: Proceedings of the International Symposium, Testing In-Situ of Concrete Structures. Budapest, 1977. 109–117
57 Malvern L E, Jenkins D A, Tang T, et al. Dynamic compressive testing of concrete. In: Proceedings of Second Symposium on the Interaction of Non-Nuclear Munitions with Structures. Florida, 1985
58 Grote D L, Park S W, Zhou M. Dynamic behavior of concrete at high strain rates and pressures: I. experimental characterization. Int J Impact Eng, 2001, 25: 869–886